10th International Conference
12-14 July 2010
Southampton
RASD 2010

THE EFFECT OF A NON-GAUSSIAN RANDOM LOADING ON HIGH-CYCLE FATIGUE OF A THERMALLY POST-BUCKLED STRUCTURE

Stephen A. Rizzi[1*], Marlana N. Behnke[2] and Adam Przekop[3]

[1]NASA Langley Research Center
Structural Acoustics Branch
Hampton, Virginia 23681 USA
E-mail: Stephen.A.Rizzi@nasa.gov

[2]Department of Mechanical and Aerospace Engineering
University of Florida
Gainesville, Florida 32611 USA
E-mail: marlanab@ufl.edu

[3]Analytical Services and Materials, Inc.
107 Research Dr.
Hampton, Virginia 23666 USA
E-mail: Adam.Przekop@nasa.gov

Keywords: Non-Gaussian loading, High-cycle fatigue

ABSTRACT

High-cycle fatigue of an elastic-plastic beam structure under the combined action of thermal and high-intensity non-Gaussian acoustic loadings is considered. Such loadings can be highly damaging when snap-through motion occurs between thermally post-buckled equilibria. The simulated non-Gaussian loadings investigated have a range of skewness and kurtosis typical of turbulent boundary layer pressure fluctuations in the vicinity of forward facing steps. Further, the duration and steadiness of high excursion peaks is comparable to that found in such turbulent boundary layer data. Response and fatigue life estimates are found to be insensitive to the loading distribution, with the minor exception of cases involving plastic deformation. In contrast, the fatigue life estimate was found to be highly affected by a different type of non-Gaussian loading having bursts of high excursion peaks.

1. INTRODUCTION

High performance aircraft structures subject to extreme thermal-acoustic loadings may exhibit geometric and material nonlinearity. These nonlinearities alter the dynamic stress response which in turn affects the high-cycle fatigue life. Previous work by the authors investigated the high-cycle fatigue of a nonlinear aluminum structure undergoing snap-through response in a thermally post-buckled condition [1]. In that work, the random pressure loading was

assumed to have a Gaussian distribution. It has been shown, however, that quasi-statically applied non-Gaussian loadings can accelerate fatigue damage accumulation [2, 3]. Therefore it is of interest to consider the effect of non-Gaussian random loadings on the fatigue of a thin-walled structure undergoing nonlinear *dynamic* response.

There has been considerable research related to non-Gaussian loading and nonlinear structures. Indeed, fatigue of offshore structures entails both non-Gaussian loading [4] and nonlinear dynamic response [5] analyses. Fatigue of thin-walled nonlinear dynamical structures subject to normally distributed loadings has received much attention [1, 6-9]. Further, the effects of non-Gaussian loadings on the nonlinear dynamic response of thin-walled structures have been investigated [10, 11], but without consideration of fatigue. There are no known studies, however, which specifically address the effects of non-Gaussian loadings on high-cycle fatigue of dynamically nonlinear thin-walled structures.

Of particular interest are non-Gaussian loadings common to high-speed flight, e.g. wall pressure fluctuations beneath a turbulent boundary layer (TBL). Recent analysis of TBL fluctuating pressures measured on the sidewall of a supersonic transport aircraft [12, 13] indicated them to be non-Gaussian [14]. In the case of a smooth sidewall, skewness and kurtosis were approximately zero and four, respectively. In the case of pressure fluctuations upstream of forward facing steps, skewness ranged between ±1, and kurtosis commonly ranged between 3 and 7. Figure 1 and Figure 2 show the long and short timescale behavior of non-Gaussian TBL data ahead of a 7 mm forward facing step at Mach 1.8. Besides skewness and kurtosis, an important characteristic of this loading is the duration of individual high excursion events and the rate of excursions. For the representative data in these figures, the typical duration of each high excursion event is on the order of 1ms, with a typical rate of high excursion peaks on the order of 600-800 per second.

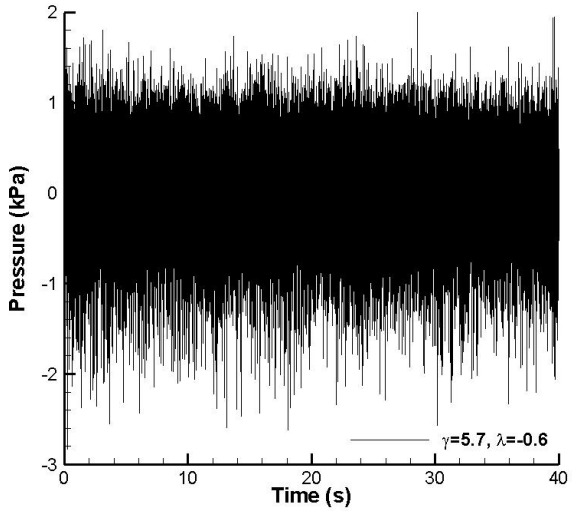

Figure 1: Long timescale behavior of non-Gaussian TBL pressure.

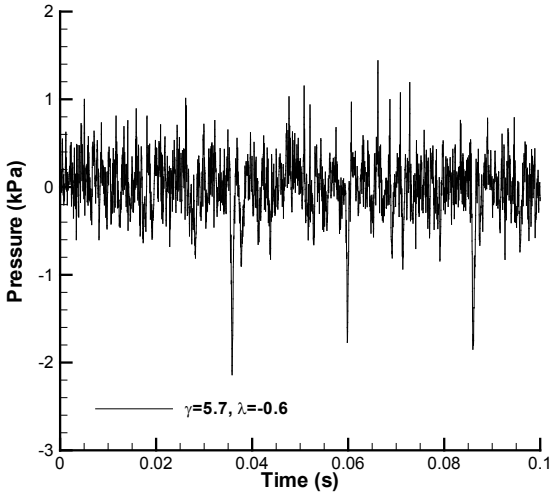

Figure 2: Short timescale behavior of non-Gaussian TBL pressure.

The goal of this work is to investigate the effects of a uniformly distributed temperature combined with a non-Gaussian acoustic loading on the dynamic response and high-cycle fatigue of a pre- and post-buckled structure. Rather than using TBL fluctuating pressure data directly, non-Gaussian TBL-like pressure loadings are generated, allowing control over the range of skewness and kurtosis considered while retaining the essential temporal characteristics indicated above. Further, records of arbitrary length can be generated to ensure converged results. A nonlinear time domain simulation in physical degrees-of-freedom is used to compute the dynamic response as both material and geometric nonlinearities are

present in the thermally pre-buckled and post-buckled regimes. Fatigue life estimates are made using a non-zero mean damage model combined with a linear cumulative damage rule.

2. NONLINEAR DYNAMIC RESPONSE SIMULATION

An aluminum beam structure previously considered [1] served as the basis for the current investigation. The beam was chosen so that long nonlinear simulations would be practical. The beam measured 457.2 mm x 25.40 mm x 2.286 mm (l x w x h), and had clamped boundary conditions at both ends, see Figure 3. Idealized elastic-plastic material properties with linear strain hardening were used, as shown in Figure 4. The elastic-plastic properties were based on empirical data and are given as: elastic modulus $E = 73.11$ GPa, shear modulus $G = 27.59$ GPa, plastic modulus $H = 417$ MPa, plastic yielding stress $\sigma_p = 400$ MPa, mass density $\rho = 2763$ kg/m^3, and coefficient of thermal expansion $\alpha = 22.32$ (μm/m)/°C. The elastic and plastic strains are ε_e and ε_p, respectively. It was assumed that the plastic modulus and yield stress are the same in tension and compression. Material properties were assumed to be temperature independent because of the modest temperature range considered in this paper. Mass proportional damping of magnitude 14.52 s^{-1} was used in all the simulations. A failure criterion, e.g., ultimate tensile strength, was not imposed on the response modeling.

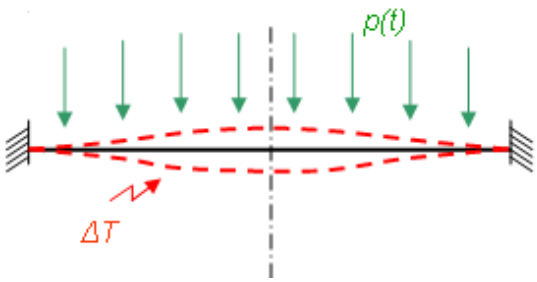

Figure 3: Beam under combined thermal-acoustic loading.

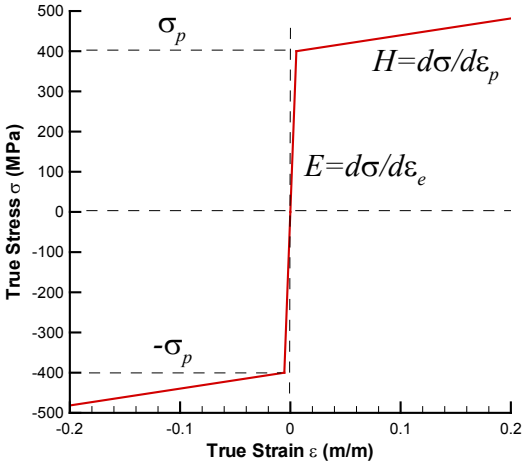

Figure 4: Elastic-plastic material properties.

The beam response was analyzed with the finite element code ABAQUS. The finite element model consisted of 144 B21 beam elements 3.175 mm long. The two node B21 element allows single-plane bending and has one rotational and two translational degrees-of-freedom (DoF) at each node. The clamped boundary conditions were modeled by constraining the rotational and both translational (transverse and in-plane) DoFs at each end of the beam.

The ABAQUS/Explicit solution was used with an automatic time step adjustment, known as 'element-by-element' in ABAQUS [15]. This approach yields a conservative time step increment. Time histories of the transverse displacement and normal stress were computed for each loading condition. Nodal displacements at the quarter-span (114.3 mm) node are subsequently shown. Because ABAQUS/Explicit computes element stresses, not nodal stresses, the normal stress was computed in proximity to the clamped boundary node at a mid-element coordinate of 1.6 mm. The normal stress on the upper and lower element surfaces was used in subsequent analyses.

2.1 Non-Gaussian acoustic loading

The principal metrics describing non-Gaussian features of the probability density function (PDF) of a random variable x are skewness λ and kurtosis γ. These are expressed in terms of the central moments of M_n of the PDF as

$$\lambda = \frac{M_3}{(M_2)^{3/2}} = \frac{M_3}{\sigma^3}, \qquad \gamma = \frac{M_4}{(M_2)^2} = \frac{M_4}{\sigma^4}. \tag{1}$$

where $\sigma^2 = M_2$ is the variance, and σ is the standard deviation. For discrete time series data, the central moments and mean m are computed from

$$M_n = \frac{1}{N}\sum_{i=1}^{N} \left[x_i - m \right]^n, \qquad m = \frac{1}{N}\sum_{i=1}^{N} x_i . \tag{2}$$

The kurtosis characterizes the sharpness of the PDF peak and the width of the PDF tails. The skewness is a measure of the asymmetry of the PDF with a positive value skewed in the negative direction. For a Gaussian distribution, $\lambda = 0$ and $\gamma = 3$. A kurtosis value greater than 3 indicates a sharper peak and wider tails relative to a Gaussian distribution.

Another indicator of non-Gaussian character is the crest factor C, defined by

$$C = \left| x \right|_{peak} \Big/ x_{rms} . \tag{3}$$

In contrast to the skewness and kurtosis, no strict theoretical value can be defined for the crest factor of a non-Gaussian process because the magnitude of the largest peak depends on the length of time history. While the skewness and kurtosis summarize the effect of all peaks that make a signal non-Gaussian, the crest factor takes into account only the largest peak. Note however that the crest factor of a narrowband Gaussian random process can be determined from the cumulative distribution function for the extreme value of a random (narrowband) process [16] as

$$C = \sqrt{2 \ln\left(-N_P \Big/ \ln\left(\rho_N \right) \right)} . \tag{4}$$

where N_P is the number of positive peaks and ρ_N is the probability of occurrence.

Based on the flight data analysis [14], four relevant non-Gaussian loading conditions were considered in addition to the Gaussian case. Nominal values are shown in bold in Table 1, along with actual values achieved by the load generation process (described in Section 2.1.1).

γ \ λ	**-0.5**	**0**	**0.5**
7	7.02/-0.51/7.89	7.15/0.00/7.38	7.20/0.47/8.02
5		4.84/-0.01/6.39	
3		2.99/0.00/4.62	

Table 1: Nominal kurtosis and skewness conditions (bold) compared with generated kurtosis/skewness/crest factor from 52 s records.

A flat spectrum between 1-1500 Hz was used in lieu of an actual TBL spectrum in order to more effectively compare the present results with the earlier work [1]. Sound pressure levels of 152 dB, 158 dB, and 170 dB (re: 20 μPa) were investigated. These seemingly high levels were obtained by scaling the smooth wall TBL level, which varied between 130-140 dB, by up to 30 dB. Such amplification was observed in the TBL ahead of forward facing steps [17]. The load was applied uniformly along the span of the beam, perpendicular to the un-deformed configuration. The method of load generation is next described.

2.1.1 Method of non-Gaussian load generation

The procedure for generating Gaussian and non-Gaussian loading time histories is fully described in [18] and is summarized here. The particular method employed uses one β-distribution to specify the phase distribution and a second β-distribution to specify the distribution of peak amplitudes. The latter was set to give a uniform distribution of peak amplitudes. In addition, since the modification of phase typically results in positive peaks, the skewness is controlled by inverting a portion of the blocks of the generated waveform. Specifically, a block inversion is made when a random number between 0 and 1 exceeds a specified threshold. An overlap-add technique ensures a smoothly varying waveform. In this manner, a β-distribution phase parameter of 1 and inversion threshold of 0.5 will generate a Gaussian time history.

The relationship between the β-distribution phase parameter and inversion threshold value, and a resulting skewness-kurtosis pair was established indirectly. Time histories were generated for discrete values of the β-distribution phase parameter in the range 1-7, and discrete values of the inversion threshold in the range 0-0.95. Each time history was computed with a 20 kHz sampling rate and record length of 2^{18} samples or approximately 13 s. From the time histories, skewness and kurtosis values were computed using equation (1). Figure 5 and Figure 6 show the variation of skewness and kurtosis with these parameters. Values for the β-distribution phase parameter and inversion threshold values closely corresponding to the nominal skewness-kurtosis pairs in Table 1 were obtained via lookup. These values were then used to generate longer record lengths, ranging from 52-150 s, for response simulation and fatigue life estimation. Table 1 also shows the actual values of kurtosis, skewness and crest factor (computed using equation (3)) obtained from 52 s time histories. Based on the observation that the number of positive peaks N_P is approximately equal to the number of positive zero crossings N_0 for a narrowband Gaussian process, equation (4) can be used to approximate the crest factor for a wideband Gaussian process when N_0 is used in place of N_P. The validity of this approximation is demonstrated for the median expected peak ($\rho_N = 0.5$) which yields a crest factor of 4.72 compared to the value of 4.62 indicated in Table 1. This assumption is valid only for the Gaussian case, as equation (4) yields essentially the same crest factor of 4.72 for the non-Gaussian cases, while the crest factor computed using equation (3) clearly shows otherwise.

The long timescale behavior of a generated non-Gaussian $(\gamma = 7, \lambda = 0.5)$ time history, normalized to 1 unit RMS, is shown in Figure 7. The frequent and steady rate of high excursions are similar in character to those observed in the non-Gaussian TBL data, see Figure 1. The short timescale record shown in Figure 8 more clearly indicates the typical rate of high excursions, each of which is approximately 0.7 ms in duration, again similar in character to the data in Figure 2. Note that the higher crest factor associated with the non-Gaussian time histories slightly reduces the level of the non-peak portions of the waveform relative to the Gaussian time history in order to maintain the same RMS level, see Figure 8. The power spectral density (PSD) of all generated time histories is virtually the same for any skewness-kurtosis pair and is shown in Figure 9. The PDFs of generated Gaussian and non-Gaussian time histories are shown in Figure 10, along with the true Gaussian PDF. The skewness, sharper peak and wider tails are evident in the non-Gaussian PDF.

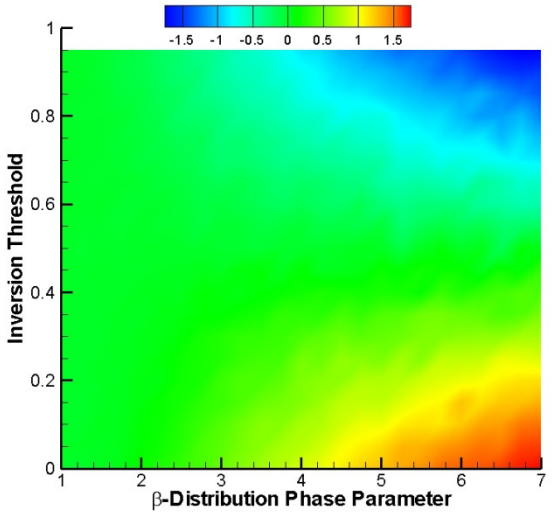

Figure 5: Variation of skewness with load generation parameters.

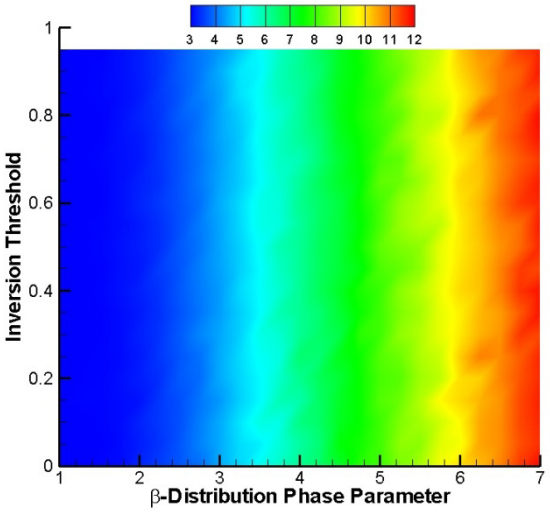

Figure 6: Variation of kurtosis with load generation parameters.

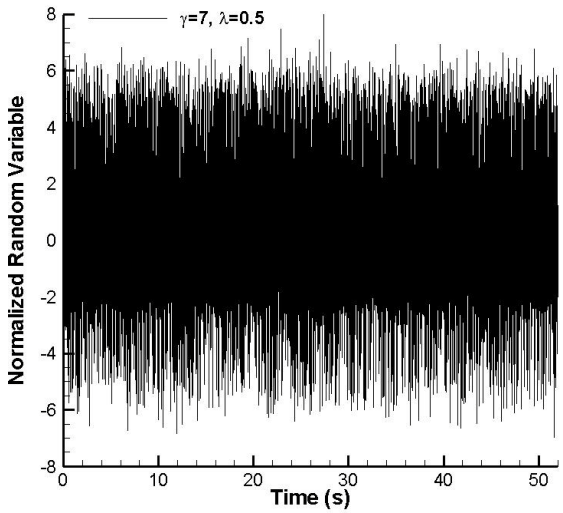

Figure 7: Long timescale behavior of a generated non-Gaussian time history.

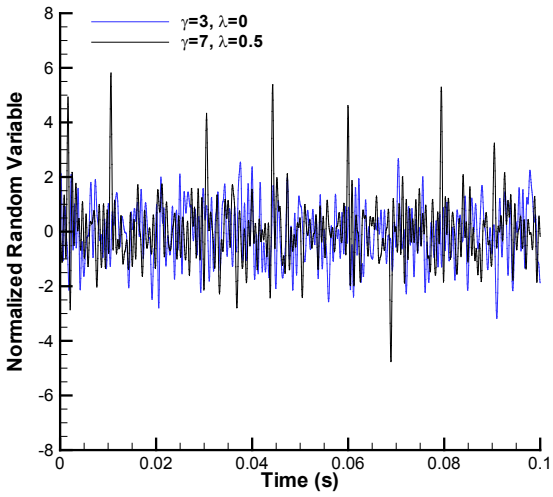

Figure 8: Short timescale behavior of a Gaussian and non-Gaussian time history.

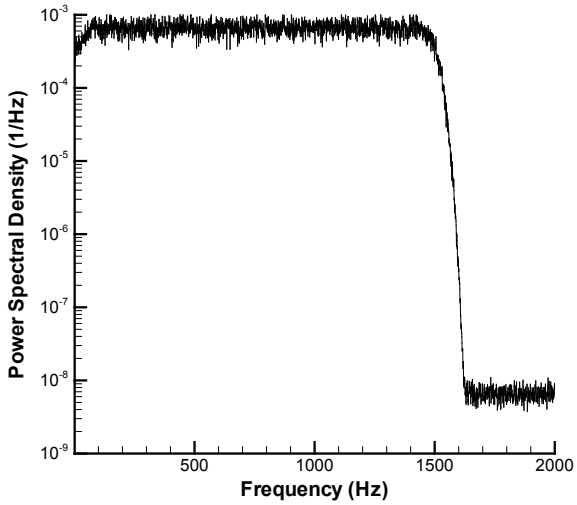

Figure 9: PSD of 52 s loading time history.

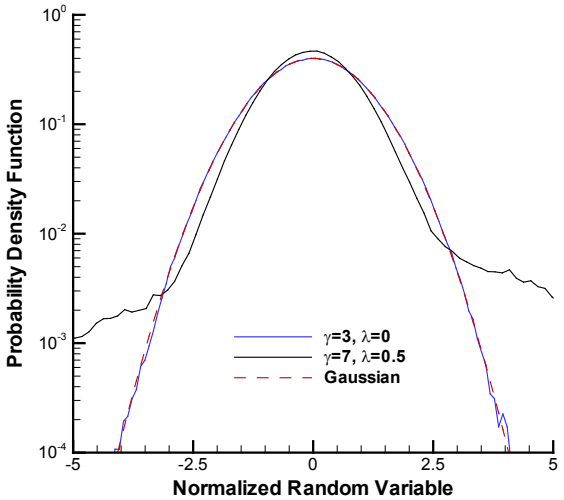

Figure 10: PDF of 52 s loading time history.

2.2 Thermal loading

To study the effect of snap-through on the dynamic response, two thermal loading conditions were considered. An ambient temperature case served as an unstressed reference condition. For this condition, a single neutral equilibrium position exists. Hence, no snap-through response was expected under any acoustic loading level under ambient temperature conditions.

The thermally post-buckled response was investigated with a uniform temperature increment of 19.44°C (35°F), well above the critical buckling temperature increment of 3.67°C (6.6°F). This condition had two non-zero symmetric equilibrium positions, as depicted by the red dashed line in Figure 3. For this condition, increasing the sound pressure level was previously shown to evolve the response from vibration around one of the positions, to intermittent snap-through and finally to persistent snap-through between the two equilibrium positions [19]. The temperature increment was applied instantaneously at the beginning of each simulation resulting in an initial transient thermal buckling response.

The combination of five non-Gaussian distributions for three sound pressure levels at two temperatures resulted in a total of thirty test cases investigated. In the remainder of the paper, these cases are specified via the shorthand notation *w*°F/*x* dB/*y*/*z*, where *w* is the temperature increment, *x* is the random pressure level, *y* is the nominal kurtosis of the pressure loading, and *z* is the nominal skewness of the pressure loading.

2.3 Simulation results

The quarter-span displacement and clamped-end surface stress PDFs of the beam subject to Gaussian and non-Gaussian loadings at ambient temperature in the linear response regime (0°F/104 dB) are shown in Figure 11 and Figure 12, respectively. Both displacement and stress response PDFs are close to Gaussian, even when the loading is non-Gaussian, see also Table 2. This is because the impulse response time of the system is long compared to the rate of high excursions. The impulse response time of the system is governed by the damping. A similar observation was made in [18, 20] for linear single degree-of-freedom systems. For more highly damped systems or for loadings with other distributions of high excursions, the same conclusion cannot be drawn. An alternative loading is considered in Section 4.

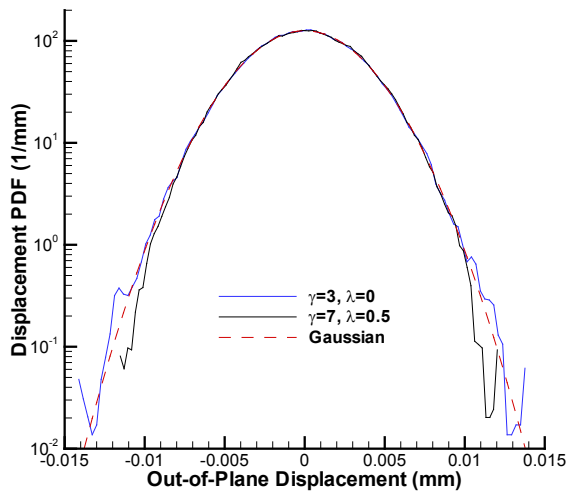

Figure 11: Displacement PDF in linear response regime (0°F/104 dB).

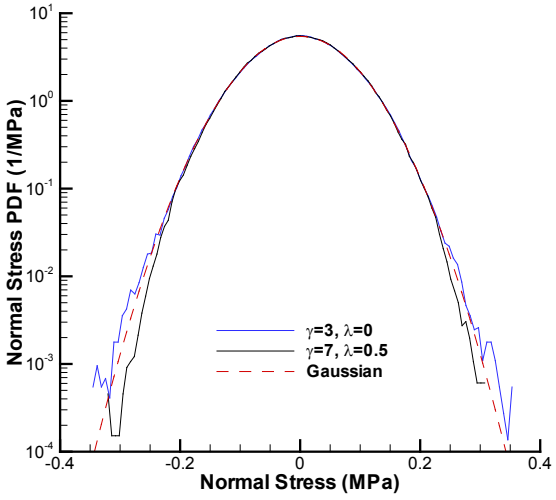

Figure 12: Normal stress PDF in linear response regime (0°F/104 dB).

Response (γ / λ)	Loading Condition			
	0°F/104 dB/3/0	0°F/104 dB/7/0.5	35°F/170 dB/3/0	35°F/170 dB/7/0.5
Displ.	3.05/0.00	2.87/0.01	2.26/0.07	2.26/-0.01
Stress	3.06/0.00	2.94/0.01	3.33/0.31	3.42/0.22

Table 2: Kurtosis and skewness of displacement and stress response for linear (0°F/104 dB) and nonlinear (35°F/170 dB) response regimes.

The quarter-span displacement and clamped-end surface stress PDFs in a nonlinear response regime (35°F/170 dB) are shown in Figure 13 and Figure 14, respectively, for Gaussian and non-Gaussian loadings. The displacement PDF takes on a bimodal character, reflecting the persistent snap-through between the two post-buckled equilibrium positions associated with this condition [1]. The surface stress PDF is skewed toward negative values due to the contribution of the membrane component, which has a compressive mean stress of approximately 46 MPa. The bending component alone has effectively zero skewness. Note also that the stress exceeds the elastic limit of 400 MPa under this loading condition. Like the linear response regime, the displacement and stress responses are not highly influenced by this particular type of loading distribution, see also Table 2. Therefore, it is anticipated that fatigue life estimates will be more affected by the system response characteristics than by the loading distribution itself.

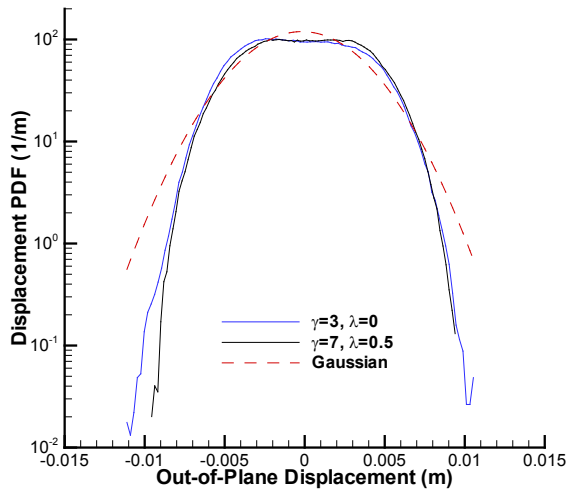

Figure 13: Displacement PDF in nonlinear response regime (35°F/170 dB).

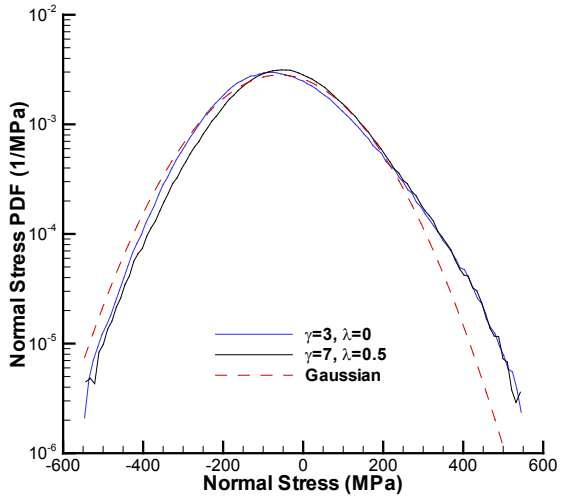

Figure 14: Normal stress PDF in nonlinear response regime (35°F/170 dB).

3. HIGH-CYCLE FATIGUE ANALYSIS

The high-cycle fatigue analysis is performed using a linear cumulative damage approach [21] with a non-zero mean damage model. The formulation is the same as previously used by the authors [1] and is summarized here. The expected damage $E[D]$ is given by

$$E[D] = \frac{T}{T_r} \sum_{-\infty}^{\infty} \sum_{-\infty}^{\infty} \frac{RFM(\sigma_{\min}, \sigma_{\max})}{N_f(\sigma_{\min}, \sigma_{\max})} \tag{5}$$

where T is the estimated median fatigue life, T_r is the record length, N_f is the number of cycles to failure for a given stress range pair $(\sigma_{\min}, \sigma_{\max})$, and the two-dimensional histogram of rainflow ranges is given by the rainflow matrix $RFM(\sigma_{\min}, \sigma_{\max})$. N_f is determined by the choice of damage model. In this paper, the *RFM* was obtained using the

Wave Analysis for Fatigue and Oceanography (WAFO) Matlab toolbox for analysis of random waves and loads [22]. Median failure occurs when $E[D]=1$, giving T as

$$T = T_r \Big/ \sum_{-\infty}^{\infty}\sum_{-\infty}^{\infty} \frac{RFM(\sigma_{\min},\sigma_{\max})}{N_f(\sigma_{\min},\sigma_{\max})} = T_r \Big/ \sum_{-\infty}^{\infty}\sum_{-\infty}^{\infty} RFD(\sigma_{\min},\sigma_{\max}) \tag{6}$$

where $RFD(\sigma_{\min},\sigma_{\max})$ is the two-dimensional rainflow damage matrix.

In order to determine the effect of non-Gaussian loading on the fatigue life, a single damage model was required for all loading conditions studied. The Walker damage model was selected as it takes into account the non-zero mean stress and was found to produce conservative fatigue life estimates over a broad range of response regimes [1]. For the Walker model, the number of cycles to failure is

$$N_{fw} = \left[\frac{\sigma_{\max}}{A_w} \left(\frac{1-R}{2} \right)^{\Gamma} \right]^{1/b_w} \tag{7}$$

where $A_w = \sigma'_{fw} 2^{b_w}$ and σ'_{fw}, b_w, and Γ are material properties determined from tests performed over a range of stress ratios $R = \sigma_{\min}/\sigma_{\max}$. Material properties used in the Walker model are [23]: σ'_{fw} = 1772 MPa, b_w = -0.163, and Γ = 0.460. It should be noted that the Walker model material data are not considered valid for R < -2, hence N_{fw} is not calculated for stress ratios in that range.

3.1 Convergence

Because the loading is random, sufficiently long stress time histories must be used to obtain converged fatigue life estimates. A method for establishing convergence is next described. The initial 1 s of response was first discarded to minimize the effects of transient behavior on the fatigue life. Next, fatigue life estimates were made for a sliding analysis block of 10 s with a hop size of 10 s. For example, a record of 52 s would yield 5 analysis blocks, i.e., 0-10 s, 10-20 s, 20-30 s, 30-40 s, and 40-50 s. The mean, minimum and maximum fatigue estimates were recorded. Next, the process was repeated with a block size of 20 s but keeping a hop size of 10 s. For the 52 s record, this would yield 4 analysis blocks of 0-20 s, 10-30 s, 20-40 s, and 30-50 s. The process was continued until the block size was maximized. The block size was determined to converge when its minimum and maximum fatigue life estimates were within 10% of the mean fatigue life estimate.

A convergence plot for the 35°F/170 dB/3/0 load condition is shown in Figure 15. The upper and lower bars for each block size represent the maximum and minimum estimates for that block size, and the symbol the mean estimate. As the block size increases, the mean can be seen to rapidly converge while the difference between maximum and minimum decreases. For this condition, convergence was achieved with a minimum block size of 70 s.

Convergence times for all loading conditions are shown in Figure 16. There appears to be no correlation of convergence time with loading distribution. All but two cases converged within 100 s, namely 35°F/152 dB/3/0 which converged after 130 s and 35°F/152 dB/5/0 which failed to converge within 150 s. The 35°F/152 dB cases had longer convergence times because the acoustic loading was high enough to cause very rare (3 or less) snap-through motions over the entire 150 s simulated response, as shown in Figure 17 for the 35°F/152 dB/5/0 loading condition. This rate of occurrence is significantly less than the intermittent snap-through condition associated with the 35°F/158 dB loading conditions, thus preventing convergence within a reasonable simulation time period.

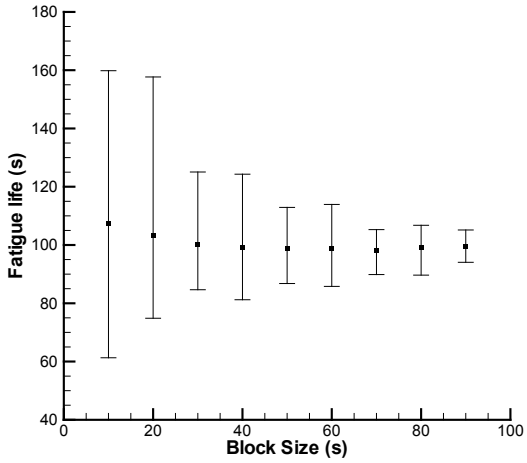

Figure 15: Convergence plot for the 35°F/170dB/3/0 loading condition.

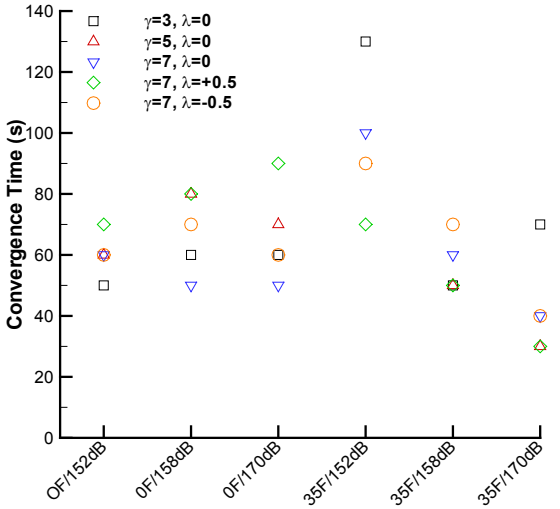

Figure 16: Convergence times for all loading conditions.

Record lengths T_r in excess of the minimum required for convergence were used in the fatigue life estimates that follow. T_r was 104 s for all but the 35°F/152 dB/3/0 case, which used a 150 s record length.

3.2 Fatigue results

Normalized fatigue life estimates at the clamped end are provided in Table 3 – Table 9 for all loading conditions. Unless otherwise noted, the estimates were made using the lower surface stress. In each case, the mean fatigue life estimate is normalized by the mean Gaussian life estimate at the corresponding thermal-acoustic loading condition. Consistent with earlier findings for Gaussian loadings [1], the fatigue life estimates are lower for the post-buckled conditions (35°F) than for ambient conditions at the corresponding sound pressure level. Variances in the fatigue life estimate greater than 10% from the Gaussian condition are highlighted in red.

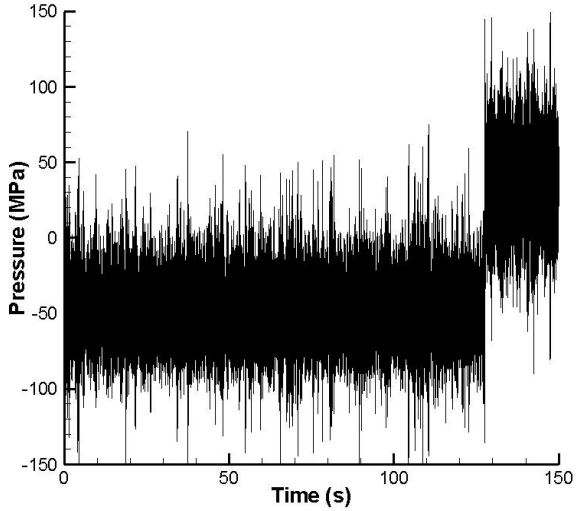

Figure 17: Lower surface stress time history for the 35°F/152 dB/5/0 loading condition.

γ \ λ	-0.5	0	0.5
7	0.92	0.93	1.28
5		1.27	
3		1.00	

Table 3: Fatigue life estimates for 0°F/152 dB conditions normalized to Gaussian life (1.40 yrs).

For the 0°F/152 dB (Table 3), 0°F/158 dB (Table 4), and 35°F/158 dB (Table 8) conditions, the variances fall largely within the above convergence criterion. The largest variance of 28% can be accounted for by a reduction in the Gaussian stress level of less than 4%. Indeed, the common industry practice of adding 3.5 dB (a 150% increase) to the applied load level would greatly outweigh any differences due to non-Gaussian loading. Further, the variances found are well below those observed between different damage models [1]. There are no apparent trends of a particular non-Gaussian loading leading to a greater or lesser fatigue life estimate relative to the Gaussian case.

γ \ λ	**-0.5**	**0**	**0.5**
7	0.83	1.04	0.82
5		0.84	
3		1.00	

Table 4: Fatigue life estimates for 0°F/158 dB conditions normalized to Gaussian life (197 hrs).

γ \ λ	**-0.5**	**0**	**0.5**
7	0.93	1.08	1.03
5		0.88	
3		1.00	

Table 5: Fatigue life estimates for 0°F/170 dB conditions normalized to Gaussian life (169 s).

γ \ λ	**-0.5**	**0**	**0.5**
7	944	0.79	0.53
5		—	
3		1.00	

Table 6: Lower surface fatigue life estimates for 35°F/152 dB conditions normalized to Gaussian life (40.5 days).

γ \ λ	**-0.5**	**0**	**0.5**
7	0.43	1.41	451
5		—	
3		1.00	

Table 7: Upper surface fatigue life estimates for 35°F/152 dB conditions normalized to Gaussian life (48.8 days).

γ \ λ	**-0.5**	**0**	**0.5**
7	1.08	1.11	0.99
5		0.92	
3		1.00	

Table 8: Fatigue life estimates for 35°F/158 dB conditions normalized to Gaussian life (38.3 hrs).

γ \ λ	**-0.5**	**0**	**0.5**
7	1.24	1.34	1.19
5		1.20	
3		1.00	

Table 9: Fatigue life estimates for 35°F/170 dB conditions normalized to Gaussian life (98.1 s).

With regard to the 35°F/152 dB loading conditions, fatigue life estimates were made for both the lower (Table 6) and upper (Table 7) surfaces as the stresses varied greatly for oscillations about either thermally post-buckled equilibrium position. For the upper equilibrium position, the lower surface has a compressive mean stress, as shown in the beginning portion of the stress time history record in Figure 17. An inspection of each stress time history revealed no correlation between the skewness of the input loading and the dominant equilibrium position. Here the dominant equilibrium position is meant to indicate the position at which the beam spends the most time. For the Gaussian case, there was no dominant equilibrium position as the beam spent a comparable amount of time in both positions. For the 35°F/152 dB/7/0 loading condition, the lower position was dominant (but not exclusive), giving the lower surface a tensile mean stress and the upper surface a

compressive mean stress. Hence, the estimated fatigue life is shorter on the lower surface than it is on the upper surface. For the 35°F/152 dB/7/0.5 loading condition, the lower position was assumed for the entire record, even though the skewness of the loading was positive. The lower surface therefore had a reduced fatigue life relative to the upper surface. For the 35°F/152 dB/7/-0.5 loading condition, the opposite was true. Because of the rare occurrences of snap-through for the 35°F/152 dB loading conditions, it is not considered appropriate to put emphasis on the variance of life from the Gaussian condition.

Finally, while the variances of fatigue life for the 0°F/170 dB and 35°F/170 dB loading conditions are similar to the other loading conditions, these conditions differ from the rest in that material nonlinearity is present. The effect of material nonlinearity alters the response due to residual stresses and limiting of high stress amplitudes in excess of the yield stress. For Gaussian loadings, material nonlinearity was previously shown to increase fatigue life estimates compared to estimates computed using a linear elastic material model [1]. This life extension, however, comes at the expense of permanent plastic deformation. Examination of the plastic strain for Gaussian and non-Gaussian conditions (not shown) indicated differences in both magnitude and areal extent. These differences had a negligible effect on the stress response for the 0°F/170 dB cases (not shown), which are characterized by large vibrations about the neutral equilibrium position, i.e., no snap-through motion. Consequently comparable fatigue life estimates were obtained for Gaussian and non-Gaussian conditions, as indicated in Table 5. The 35°F/170 dB cases are characterized by large vibrations about two non-zero equilibrium positions with persistent snap-through. For these cases, the fatigue life estimate for the Gaussian loading condition was found to be somewhat lower than all of the non-Gaussian loadings, see Table 9. Here, the combined effect of material and geometric nonlinearity resulted in a slight (3-4%) reduction of the dynamic stress response of the non-Gaussian conditions relative to the Gaussian condition. This is evidenced in the rainflow matrices. The rainflow matrix for the Gaussian loading, shown in Figure 18, indicates a peak stress range of 610 MPa, while a representative non-Gaussian condition (35°F/170 dB/7/0) shown in Figure 19 indicates a peak stress range of 590 MPa. Since most of the damage occurs at the high stress ranges, the fatigue life estimate for the Gaussian loading condition is shorter than the non-Gaussian cases.

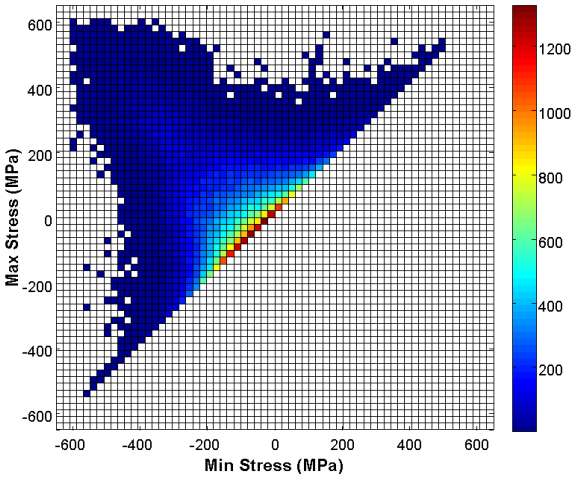

Figure 18: Rainflow matrix for 35°F/170 dB/3/0 loading condition.

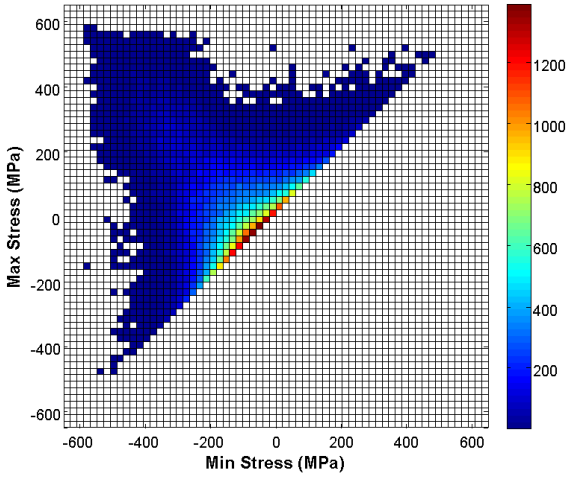

Figure 19: Rainflow matrix for 35°F/170 dB/7/0 loading condition.

4. OTHER NON-GAUSSIAN LOADINGS

It is useful to consider other non-Gaussian loadings with characteristics different than those typical of TBL to give a broader perspective on the effects of non-Gaussian loads on high-cycle fatigue life. Of particular interest are non-Gaussian loadings where the rate of high excursion events is longer than the system impulse response time, such as might be encountered in unsteady separated flows.

A method for generating such loadings uses a β-distribution to modulate the amplitude window, as described in [18]. This method allows control over kurtosis, but is limited to zero skewness. The long timescale behavior of a generated non-Gaussian $(\gamma = 7, \lambda = 0)$ time history, normalized to 1 unit RMS, using this approach is shown in Figure 20. Here, the same flat spectrum between 1-1500 Hz was specified. The actual values of kurtosis, skewness and crest factor (using equation (3)) are 6.88, -0.02, and 9.21, respectively. Unlike the approach which uses a β-distribution to specify the phase and peak amplitude distributions (see Section 2.1.1), modulation of the amplitude window results in a time history with relatively long bursts of high amplitudes. A time history of the number of peaks in excess of 3σ for non-overlapping 0.5 s blocks is shown in Figure 21. The variation is substantial, from zero to over 2000. In contrast, the same quantity using the method of Section 2.1.1 gives a relatively steady rate of about 300 peaks per block over the entire time history, and is more representative of TBL data. The corresponding PDFs shown in Figure 22 are substantially different and further demonstrate that spectrum and kurtosis specification alone are insufficient to characterize the random loading.

The effect of this alternative load generation approach on the fatigue life is considered for the 35°F/158 dB/7/0 loading condition. The PDF of the positive stress peaks corresponding to both non-Gaussian loadings is shown in Figure 23, normalized to a stress standard deviation of about 55.5 MPa in each case. The TBL-like loading generated with the β-phase method follows the Gaussian peak PDF for the positive stresses. However, the peak stress PDF for the alternative loading generated with the window amplitude modulation method exhibits much higher peak stresses. It is the positive peak stresses that account for most of the fatigue damage. Consequently, the fatigue life estimate of 9.29 hrs for the alternative loading is 4.13 times less than that of the Gaussian condition. This is a significant difference compared to the TBL-like loading which had a fatigue life estimate comparable (92%) to that of the Gaussian condition.

The cumulative distribution function (CDF) of the positive stress peaks may be evaluated to lend insight into the convergence of fatigue life estimates. The positive stress peak CDF, shown in Figure 24 for the high probability values, indicates that the TBL-like loading generated with the β-phase method has a higher cumulative probability than the alternative loading above 2σ. For example, the cumulative probability of a 3σ positive stress peak is 99.84% for the TBL-like loading and is 99.38% for the alternative loading. Therefore, longer time histories are required to realize high σ events when using the alternative loading (window amplitude modulation method) than when using the TBL-like loading (β-phase load generation method). This is borne out in the extended time (170 s) required for fatigue life convergence using the alternative loading, compared to a shorter time (60 s) required for the TBL-like loading, see Figure 25. Note also that the ratio of maximum to minimum fatigue life estimate for this loading is much larger for small block sizes than it is for the TBL-like loading. For a block size of 10 s, for example, the ratio of maximum to minimum fatigue life exceeds 40 for this loading, and is less than 3 for the TBL-like loading.

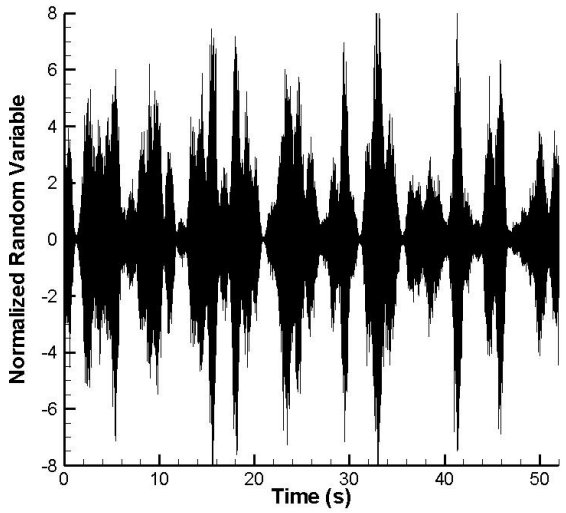

Figure 20: Time history of non-Gaussian loading using window amplitude modulation.

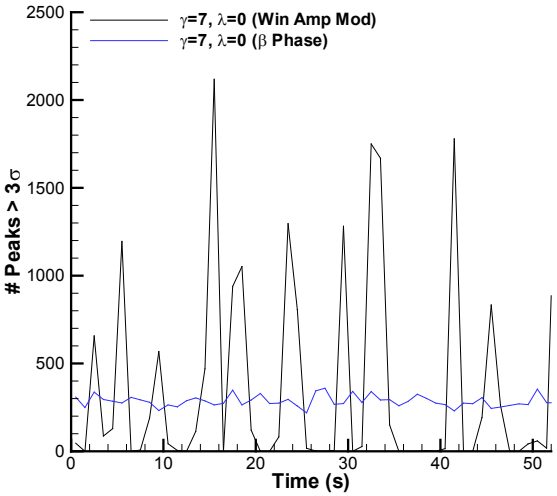

Figure 21: Peak time history of non-Gaussian loadings obtained with two different methods.

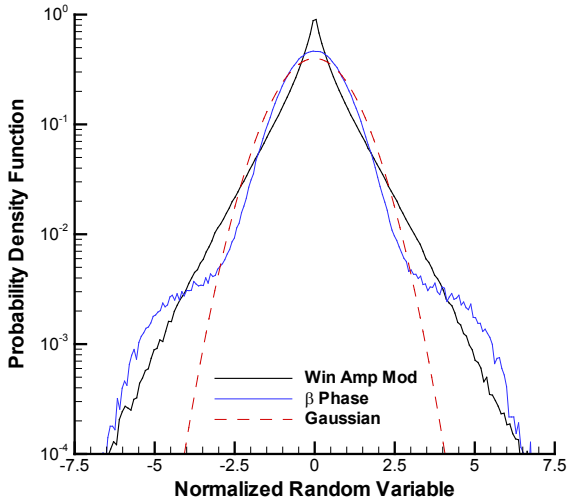

Figure 22: PDF of two non-Gaussian loadings, see Figure 21.

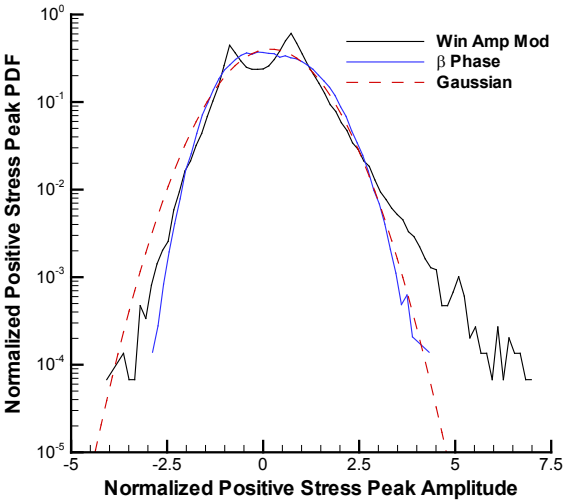

Figure 23: Normalized positive stress peak PDF due to two non-Gaussian loadings.

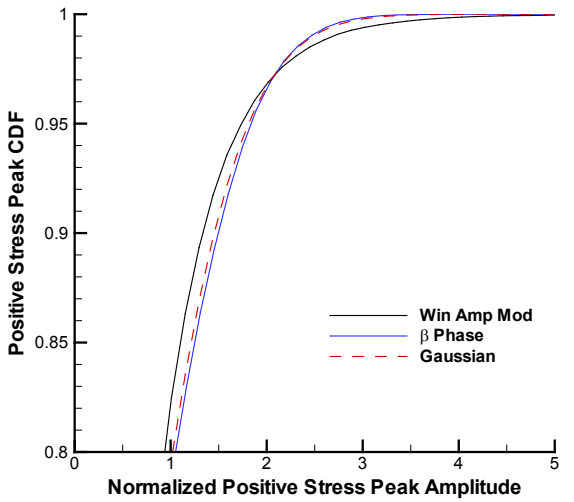

Figure 24: Normalized positive stress peak CDF due to two non-Gaussian loadings.

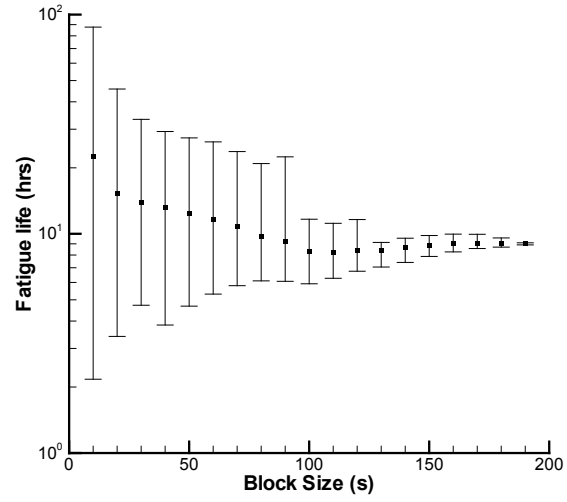

Figure 25: Convergence plot for the 35°F/158 dB/7/0 loading condition.

5. CONCLUSIONS

A study was undertaken to investigate the nonlinear response and fatigue of a pre- and post-thermally buckled structure subject to non-Gaussian random excitation. The excitation was generated to have characteristics similar to those found in pressure fluctuations beneath turbulent boundary layers.

It was found that such non-Gaussian loadings, with high and uniform rates of peak excursions, produced nearly Gaussian responses in the pre-buckled linear response regime. Here the impulse response time of the system was long compared to the rate of high excursions. In the pre- and post-buckled nonlinear response regime, the effects of geometric and material nonlinearity were more important than the loading distribution. Consequently, fatigue life estimates for all Gaussian and non-Gaussian loadings were comparable and well within customarily applied margins for loading uncertainty and variances between damage models. For cases involving material nonlinearity, the magnitude and extent of the plastic area differed between Gaussian and non-Gaussian loadings. These differences however did not significantly affect the estimated fatigue lives.

The dependency of the response and fatigue on the relationship between the impulse response time of the system and the rate of high excursions was additionally investigated by considering a second form of non-Gaussian loading, having similar kurtosis to the TBL-like loading, but with long bursts of high amplitude excursions. This loading resulted in a significantly reduced fatigue life compared to the Gaussian case. Future work may further investigate this dependency by varying the system damping in order to change the system impulse response. In this manner, attributes of both the structure and the loading may be considered in the determination of analysis requirements.

ACKNOWLEDGMENTS

The authors wish to thank David O. Smallwood (Sandia National Laboratories, retired) for guidance and use of his non-Gaussian Matlab codes, and Karl Sweitzer (ITT Geospatial Systems) for helpful discussions.

REFERENCES

[1] Przekop, A., Rizzi, S.A., and Sweitzer, K.A., "An investigation of high-cycle fatigue models for metallic structures exhibiting snap-through response," *International Journal of Fatigue*, Vol. 30, No. 9, pp. 1579-1598, 2008.

[2] Sarkani, S., Kihl, D.P., and Beach, J.E., "Fatigue of welded joints under narrowband non-Gaussian loadings," *Probabilistic Engineering Mechanics*, Vol. 9, pp. 179-190, 1994.

[3] Sarkani, S., Michaelov, G., Kihl, D.P., and Beach, J.E., "Fatigue of welded steel joints under wideband loadings," *Probabilistic Engineering Mechanics*, Vol. 11, pp. 221-227, 1996.

[4] Rychlik, I., Johannesson, P., and Leadbetter, M.R., "Modelling and statistical analysis of ocean-wave data using transformed Gaussian processes," *Marine Structures*, Vol. 10, pp. 13-47, 1997.

[5] Brouwers, J.J.H., "Nonlinear vibrations of offshore structures under random wave excitation," *Acta Applicandae Mathematicae*, Vol. 5, No. 1, pp. 1-26, 1986.

[6] Sun, J.Q. and Miles, R.N., "Acoustic fatigue life prediction for non-linear structures," *Journal of Sound and Vibration*, Vol. 150, No. 3, pp. 531-535, 1991.
[7] Sun, J.Q., Bao, W., and Miles, R.N., "Fatigue life prediction of nonlinear plates under random excitations," *Journal of Vibration and Acoustics*, Vol. 120, pp. 353-360, 1998.
[8] Sun, J.Q., Wang, X., and Bergman, L.A., "Fatigue analysis of non-linear structures with von Mises stress," *Journal of Sound and Vibration*, Vol. 245, No. 5, pp. 947-952, 2001.
[9] Sweitzer, K.A., "Random vibration response statistics for fatigue analysis of nonlinear structures," *Ph.D. Dissertation*, Institute of Sound and Vibration Research, University of Southampton, 2006.
[10] Steinwolf, A., Ferguson, N.S., and White, R.G., "Variations in steepness of the probability density function of beam random vibration," *European Journal of Mechanics - A/Solids*, Vol. 19, pp. 319-341, 2000.
[11] Antonini, A., Gioffrè, M., and Gusella, V., "Geometrically nonlinear cantilever under stochastic loading vectors," *Nonlinear Dynamics*, Vol. 28, pp. 83-102, 2002.
[12] Rizzi, S.A., Rackl, R.G., and Andrianov, E.V., "Flight test measurements from the Tu-144LL structure/cabin noise follow-on experiment," NASA TM-2000-209859, February 2000.
[13] Rizzi, S.A., Rackl, R.G., and Andrianov, E.V., "Flight test measurements from the Tu-144LL structure/cabin noise experiment," NASA TM-2000-209858, January 2000.
[14] Steinwolf, A. and Rizzi, S.A., "Non-gaussian analysis of turbulent boundary layer fluctuating pressure on aircraft skin panels," *AIAA Journal of Aircraft*, Vol. 43, No. 6, pp. 1662-1675, 2006.
[15] "ABAQUS online documentation, ABAQUS analysis user's manual." Providence, RI: Dassault Systemes Simulia Corp., 2009.
[16] Sarafin, T.P., Harmel, T.A., and Richard W. Webb, J., "Verification Criteria," In *Spacecraft Structures and Mechanisms – From Concept to Launch*, Sarafin, T.P. and Larson, W.J., Eds., Micrososm, Inc. & Kluwer Academic Publishers, 1995.
[17] Efimtsov, B.M., Golubev, A.Y., Rizzi, S.A., Andersson, A.O., Rackl, R.G., and Andrianov, E.V., "Influence of small steps on wall pressure fluctuation spectra measured on TU-144LL flying laboratory," *Proceedings of the 8th AIAA/CEAS Aeroacoustics Conference*, AIAA-2002-2605, Breckenridge, CO, June 17-19, 2002.
[18] Smallwood, D.O., "Vibration with non-Gaussian noise," *Journal of the Institute of Environmental Sciences and Technology*, Vol. 52, No. 3, pp. 13-30, 2009.
[19] Przekop, A. and Rizzi, S.A., "Dynamic snap-through of thermally buckled structures by a reduced order method," *AIAA Journal*, Vol. 45, No. 10, pp. 2510-2519, 2007.
[20] Steinwolf, A. and Ibrahim, R.A., "Numerical and experimental studies of linear systems subjected to non-Gaussian random excitations," *Probabilistic Engineering Mechanics*, Vol. 14, pp. 289-299, 1999.
[21] Miner, M.A., "Cumulative damage in fatigue," *Trans. ASME, Journal of Applied Mechanics*, Vol. 67, pp. A159-A164, 1945.
[22] "WAFO - A Matlab toolbox for analysis of random waves and loads," Version 2.1.1, The WAFO Group, Lund Institute of Technology, Lund University, 2005.
[23] Dowling, N.E., "Mean stress effects in stress-life and strain-life fatigue," *Fatigue 2004: Second SAE Brasil Conference on Fatigue*, SAE 2004-01-2227, São Paulo, Brasil, June, 2004.